40 Gb/s silicon photonics modulator for TE and TM polarisations

F. Y. Gardes,* D. J. Thomson, N. G. Emerson and G. T. Reed

Advanced Technology Institute, University of Surrey
Guildford, Surrey, GU2 7XH, UK
**f.gardes@surrey.ac.uk*

Abstract: A key device in future high speed short reach interconnect technology will be the optical modulator. These devices, in silicon, have experienced dramatic improvements over the last 6 years and the modulation bandwidth has increased from a few tens of MHz to over 30 GHz. However, the demands of optical interconnects are significant. Here we describe an approach based on a self-aligned wrap around p-n junction structure embedded in a silicon waveguide that can produce high-speed optical phase modulation, whilst at the same time, capable of a high extinction ratio. An all-silicon optical modulator using a CMOS compatible fabrication process with a data rate of 40 Gb/s and extinction ratio up to approximately 6.5 dB for TE and TM polarisations is demonstrated. This technology is not only compatible with conventional complementary MOS (CMOS) processing, but is also intended to simplify and improve the reliability of, the fabrication process.

OCIS codes: (250.7360) Waveguide modulators; (230.2090) Electro-optical devices; (250.5300) Photonic integrated circuits.

References and links

1. G. T. Reed, and A. P. Knights, *Silicon Photonics: An Introduction* (John Wiley & Sons, Inc., 2004).
2. F. Y. Gardes, G. T. Reed, N. G. Emerson, and C. E. Png, "A sub-micron depletion-type photonic modulator in silicon on insulator," Opt. Express **13**, 2005.
3. A. Liu, L. Liao, D. Rubin, H. Nguyen, B. Ciftcioglu, Y. Chetrit, N. Izhaky, and M. Paniccia, "High-speed optical modulation based on carrier depletion in a silicon waveguide," Opt. Express **15**(2), 660–668 (2007).
4. L. Liao, A. Liu, D. Rubin, J. A. B. J. Basak, Y. A. C. Y. Chetrit, H. A. N. H. Nguyen, R. A. C. R. Cohen, N. A. I. N. Izhaky, and M. A. P. M. Paniccia, "40 Gbit/s silicon optical modulator for highspeed applications," Electron. Lett. **43**, 2007.
5. D. Marris-Morini, X. Le Roux, L. Vivien, E. Cassan, D. Pascal, M. Halbwax, S. Maine, S. Laval, J. M. Fédéli, and J. F. Damlencourt, "Optical modulation by carrier depletion in a silicon PIN diode," Opt. Express **14**(22), 10838–10843 (2006).
6. C. Gunn, "CMOS Photonics for High-Speed Interconnects," Micro. IEEE **26**(2), 58–66 (2006).
7. J. W. Park, J.-B. You, I. G. Kim, and G. Kim, "High-modulation efficiency silicon Mach-Zehnder optical modulator based on carrier depletion in a PN Diode," Opt. Express **17**(18), 15520–15524 (2009).
8. P. Dong, S. Liao, D. Feng, H. Liang, D. Zheng, R. Shafiiha, C.-C. Kung, W. Qian, G. Li, X. Zheng, A. V. Krishnamoorthy, and M. Asghari, "Low Vpp, ultralow-energy, compact, high-speed silicon electro-optic modulator," Opt. Express **17**(25), 22484–22490 (2009).
9. J.-B. You, M. Park, J.-W. Park, and G. Kim, "12.5 Gbps optical modulation of silicon racetrack resonator based on carrier-depletion in asymmetric p-n diode," Opt. Express **16**(22), 18340–18344 (2008).
10. F. Y. Gardes, A. Brimont, P. Sanchis, G. Rasigade, D. Marris-Morini, L. O'Faolain, F. Dong, J. M. Fedeli, P. Dumon, L. Vivien, T. F. Krauss, G. T. Reed, and J. Martí, "High-speed modulation of a compact silicon ring resonator based on a reverse-biased pn diode," Opt. Express **17**(24), 21986–21991 (2009).
11. A. Narasimha, S. AbdaIla, C. Bradbury, A. Clark, J. Clymore, J. Coyne, A. Dahl, S. Gloeckner, A. Gruenberg, D. Guckenberger, S. Gutierrez, M. Harrison, D. Kucharski, K. Leap, R. LeBlanc, V. Liang, M. Mack, D. Martinez, G. Masini, A. Mekis, R. Menigoz, C. Ogden, M. Peterson, T. Pinguet, J. Redman, J. Rodriguez, S. Sahni, M. Sharp, T. J. Sleboda, D. Song, V. Wang, B. Welch, J. Witzens, W. Xu, K. Vokoyama, and P. De DobbeIaere, "An ultra low power CMOS Photonics Technology Platform for H/S Optoelectronic Transceivers at less than $1per Gbps," in *OFC, 22–25 March*, San Diego, USA 2010.
12. L. Tsung-Yang, A. Kah-Wee, F. Qing, S. Jun-Feng, X. Yong-Zhong, Y. Ming-Bin, L. Guo-Qiang, and K. Dim-Lee, "Silicon Modulators and Germanium Photodetectors on SOI: Monolithic Integration, Compatibility, and Performance Optimization," IEEE Sel. Top. Quan. Electron. **16**, 307–315.

#144401 - $15.00 USD Received 18 Mar 2011; revised 17 May 2011; accepted 25 May 2011; published 2 Jun 2011

13. N.-N. Feng, S. Liao, D. Feng, P. Dong, D. Zheng, H. Liang, R. Shafiiha, G. Li, J. E. Cunningham, A. V. Krishnamoorthy, and M. Asghari, "High speed carrier-depletion modulators with 1.4V-cm V(pi)L integrated on 0.25microm silicon-on-insulator waveguides," Opt. Express **18**(8), 7994–7999 (2010).
14. D. M. Gill, M. Rasras, T. Kun-Yii, C. Young-Kai, A. E. White, S. S. Patel, D. Carothers, A. Pomerene, R. Kamocsai, C. Hill, and J. Beattie, "Internal Bandwidth Equalization in a CMOS-Compatible Si-Ring Modulator," IEEE Photon. Technol. Lett. **21**(4), 200–202 (2009).
15. S. J. Spector, M. W. Geis, M. E. Grein, R. T. Schulein, J. U. Yoon, D. M. Lennon, F. Gan, G. R. Zhou, F. X. Kaertner, and T. M. Lyszczarz, "High-speed silicon electro-optical modulator that can be operated in carrier depletion or carrier injection mode," in *2008 Conference on Quantum Electronics and Laser Science Conference on Lasers and Electro-Optics, CLEO/QELS*, San Jose, CA, United states, 2008.
16. D. J. Thomson, F. Y. Gardes, G. T. Reed, F. Milesi, and J.-M. Fedeli, "High speed silicon optical modulator with self aligned fabrication process," Opt. Express **18**(18), 19064–19069 (2010).
17. D. Miller, "Device Requirements for Optical Interconnects to Silicon Chips," Proc. IEEE **97**(7), 1166–1185 (2009).

1. Introduction

An optical modulator is a device that is used to modulate a light beam that propagates either in free space or in an optical waveguide. These devices can alter different beam parameters and so can be categorized as amplitude, phase, or polarisation modulators. Furthermore, modulators can be also classified into one of two operational categories: electro-refractive or electro-absorptive.

The application of an electric field to a material can result in a change to the real and imaginary refractive indices. A change in real refractive index, Δn, with an applied electric field is known as electro-refraction, whereas a change in the imaginary part of refractive index, $\Delta\alpha$, with applied electric field is known as electro-absorption. The most common modulation method used in silicon devices to date is the plasma dispersion effect, in which the concentration of free charges in silicon changes the real and imaginary parts of the refractive index via the absorption coefficient [1]. Electrical control of the charge density, interacting with the propagating light, is achievable through mechanisms such as carrier injection, either accumulation or depletion.

In 2005 Gardes et al. proposed a modulator incorporated in a submicrometer waveguide, which for the first time, made use of the depletion mechanism . Modelling data predicted an unprecidented intrinsic bandwidth of 50 GHz [2]. The device featured a horizontal p-n junction across the waveguide with highly doped regions required for the formation of resistive contacts placed at the extremities of the waveguide to avoid excessive optical loss. Two years later a similar design was realised by Liu et al. from Intel [3]. The authors reported data transmission at 30 Gb/s [3] and later improved on this figure, demonstrating data transmission at 40 Gb/s [4]. These devices however, were only demonstrated to operate for TE polarisation and the fabrication process was relatively complex (includes processes such as epitaxial growth) . Further to this work, a plethora of carrier depletion based modulators, compatible with data transmission at speeds of at least 10 Gb/s, were demonstrated [5–16]; the Intel device [4] however, is currently the fastest silicon optical modulator reported to date.

2. Device design and fabrication

The device described in this paper is a carrier depletion based optical modulator embedded in a silicon waveguide. Figure 1 is a schematic representation of a rib waveguide incorporating a modulator, comprising an n type region wrapped around a p type region to form a p-n diode structure, both regions being located in the waveguiding area.

#144401 - $15.00 USD Received 18 Mar 2011; revised 17 May 2011; accepted 25 May 2011; published 2 Jun 2011

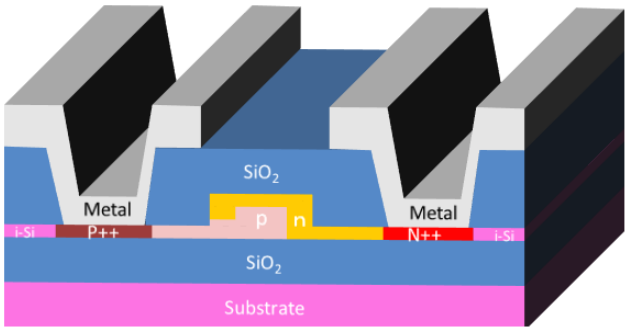

Fig. 1. Cross section of the optical modulator; illustrates the junction positioning.

A photograph, obtained from scanning electron microscopy (SEM), Fig. 2, shows the vias where the metal stack connects to the highly doped regions to form resistive contacts on both sides of the rib waveguide, at the junction location. Both p and n type regions have doping concentrations, predicted by simulation, to be around $1x10^{18}$ /cm^3 whereas the highly doped regions, both sides of the rib, are designed for a concentration of the order, $1x10^{20}$ /cm^3.

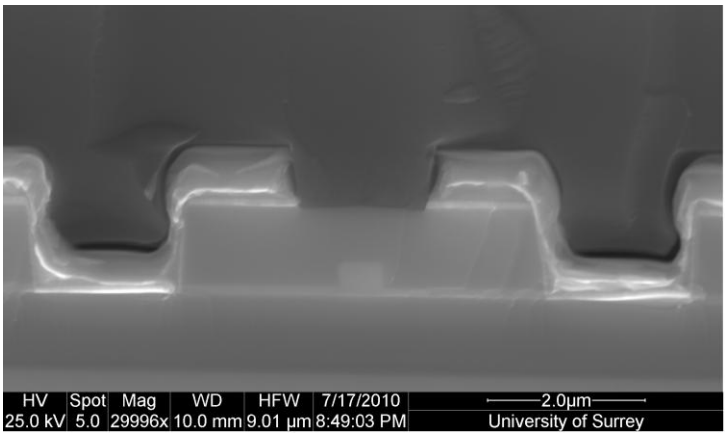

Fig. 2. SEM Cross section of the optical modulator

The diode is inserted into a single mode rib waveguide, with dimensions, height based on a 400 nm silicon overlayer, depth, defined by a 300 nm etch, and a width of 410 nm. The fabrication process used to form the doped areas relies on five self-aligned photolithographic steps where ion implantation of phosphorus and boron is used to form the active areas of the device as shown Fig. 3. The waveguide is fabricated using a traditional technique based on reactive ion etching of silicon. The process is then completed by covering the waveguiding area with one micrometer of silicon dioxide, followed by an oxide etch to open the vias; a metal stack is finally formed by metal deposition and layer patterning. The self-aligned nature of the fabrication process is predicted to improve the uniformity of device performance across a wafer. The process described in this paper avoids some of the complex steps reported elsewhere [4], such as epitaxial growth, epitaxial lateral overgrowth (ELO) and chemical mechanical polishing (CMP); hence the relative simplicity of the process should impact on the cost of device fabrication.

To convert the phase modulation into intensity modulation, we have utilised an asymmetric Mach Zehnder interferometer (MZI) and inserted the pn junction phase shifter into one arm of the MZI. A similar structure is also inserted into the other arm to balance the loss but this device is not driven during modulation. The asymmetric MZI has an optical path length difference of 80 micrometers between the two arms and a star coupler junction is used to split and recombine the optical beam in the MZI.

#144401 - $15.00 USD Received 18 Mar 2011; revised 17 May 2011; accepted 25 May 2011; published 2 Jun 2011

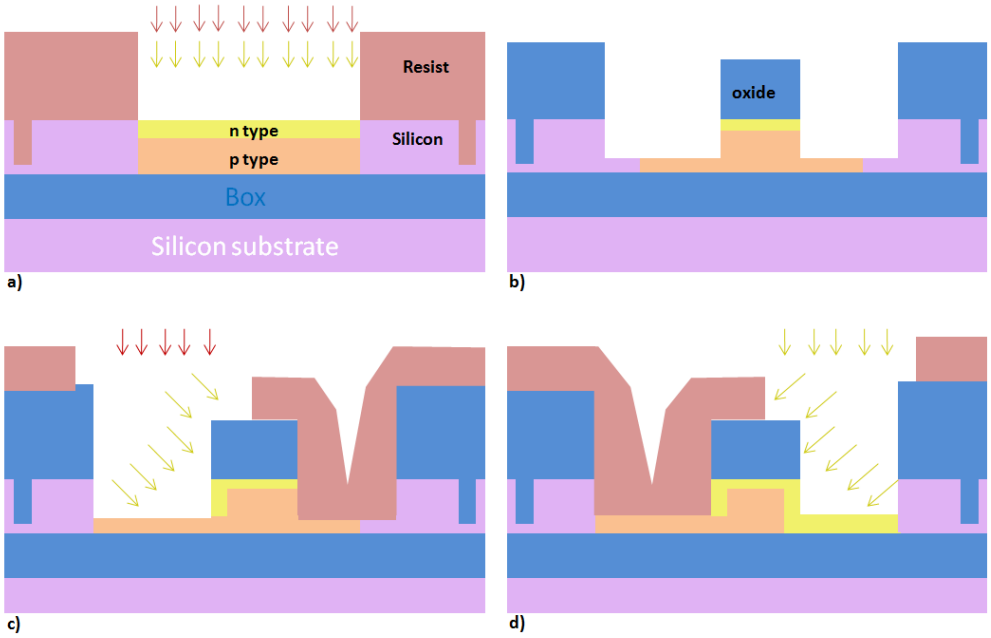

Fig. 3. Implantation process used to achieve the wrap around junction a) implantation of the horizontal junction, b) etch of the rib waveguide, c) implantation of the left side of the n type region of the rib waveguide and slab d) implantation of the right side of the n type region of the rib waveguide and slab

3. Device characterisation

To characterise the performance of the silicon MZI modulator, the optical transmission of the MZI was scanned over a wavelength range of 50 nm between 1530 nm and 1580 nm. An increasing dc reverse bias was applied to the phase shifter for each wavelength scan. The results are shown Fig. 4 and Fig. 5 for TE and TM polarizations respectively. It can also be seen from Fig. 4 and 5 that the 6 V DC extinction ratio of the MZI modulator is >8 dB in the 1555 nm region for the phase shifter of interest (effective length 1350 μm). The efficiency $V_{\pi}.L_{\pi}$ (voltage-Length required to achieve a π phase shift for a given length) extracted from the transmission shift against reverse voltage for TE and TM polarisations is ~11 V.cm and ~14 V.cm. The on-chip insertion loss is ~15 dB when the MZI is in the "on" state, which is defined here as the maximum optical output intensity of the MZI. This on-chip insertion loss (excluding coupling loss) includes ~5.7 dB and 6.7 dB of passive waveguide transmission loss for TE and TM polarisations respectively, consisting of the tapers, the 9000 micrometer long access waveguides (which are 3 micrometers wide) and the optical splitters.

#144401 - $15.00 USD Received 18 Mar 2011; revised 17 May 2011; accepted 25 May 2011; published 2 Jun 2011

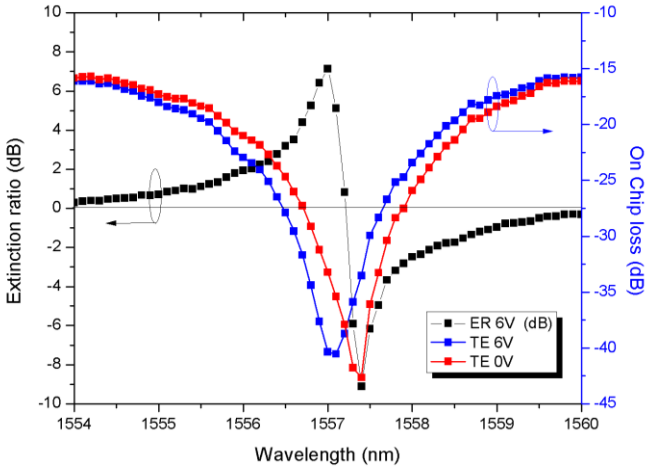

Fig. 4. On chip loss and DC extinction ratio for a phase shifter length of 1350 micrometers, at 0 V and 6 V reverse bias, for TE polarisation.

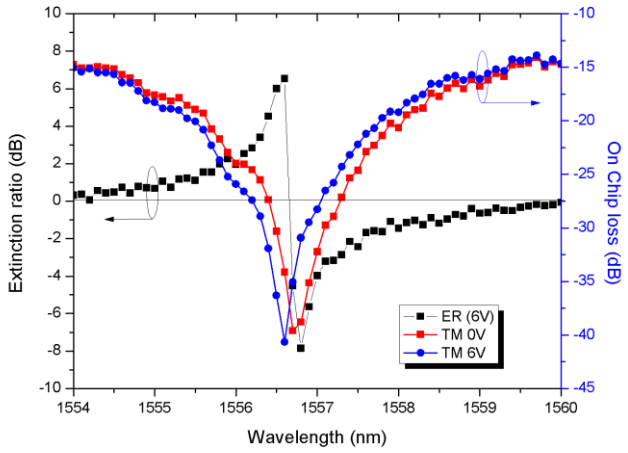

Fig. 5. On chip loss and DC extinction ratio for a phase shifter length of 1350 micrometers, at 0 V and 6 V reverse bias, for TM polarisation.

A total waveguide propagation loss for TE and TM polarisations of ~1.5 dB and 1.9 dB respectively was measured for the 410 nm wide passive waveguide sections outside of the phase shifter devices themselves. Therefore, the insertion loss of the phase shifter in isolation is only ~7.7 dB and 5.4 dB (for TE and TM polarisations respectively) for the 1350 micrometer long device. The passive waveguide loss was estimated at 0.7 dB/mm for TE and 0.9 dB/mm for TM polarisations, which is much higher than expected. This was due to etching issues creating increased sidewall roughness which has now been resolved and should improve loss figures in future iterations. The loss due to the doping in the waveguides was estimated to be approximately 5.7 dB/mm for TE and 4 dB/mm for TM polarisations, and is responsible for the majority of the phase shifter insertion loss. The loss is due to the doping level in the range of 1E18 cm^{-3} for the p and n type regions but also to the proximity of the highly doped regions located in the slab on both sides of the rib waveguide with a concentration of 1E20 cm^{-3}. The speed of the device is tightly linked to the capacitance of the junction and the resistance, and if highly doped regions located next to the junction decrease

#144401 - $15.00 USD Received 18 Mar 2011; revised 17 May 2011; accepted 25 May 2011; published 2 Jun 2011

the resistance they also impact the optical loss. Therefore careful engineering of these regions is critical to enable acceptable optical loss while retaining low resistance. Thus we can vary the design for a given application.

It is worth noting that the performance of the phase shifter is very similar for both TE and TM polarisations, which is clearly an advantage.

I-V measurements have also been performed on phase shifters of 3 different lengths which indicate a breakdown voltage of approximately 9 V. This shows that the diode can be operated up to a reverse voltage of 6-7 volts whilst avoiding reverse breakdown and the detrimental effects of high reverse leakage, as shown in Fig. 6.

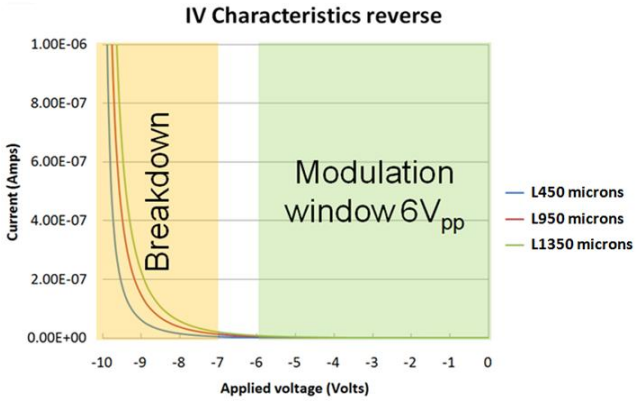

Fig. 6. Current against voltage (IV) characteristics in the reverse regime of the diode. This shows the 6 V available for the operation of the device. Above 7 V the diode reverse current increases rapidly with a breakdown voltage located around 9 V.

To operate the device at high frequency a 50 ohm coplanar waveguide (CPW) has been designed to drive the phase shifters. The central electrode is 5 micrometers wide and the separation between the signal track and ground planes is 5 micrometers. The schematic of the electrode design is shown in Fig. 7.

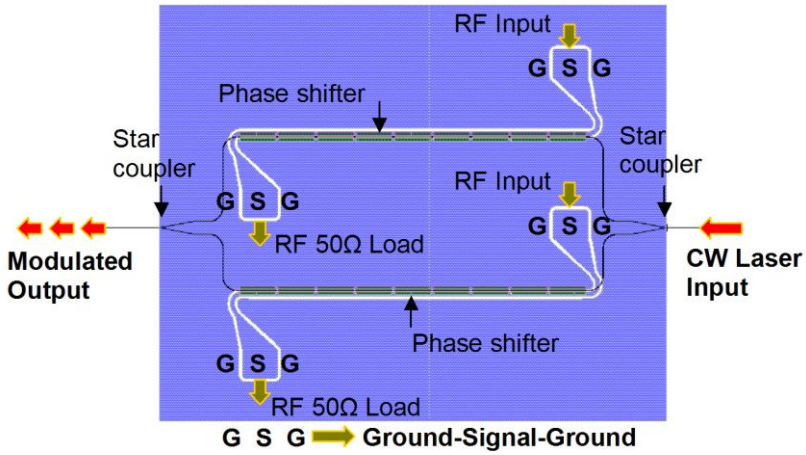

Fig. 7. Top down view of the coplanar waveguide electrode design and waveguide positioning to form a Mach Zehnder interferometer.

Transmission (S_{21}) parameters have been measured on the unloaded CPW as shown on Fig. 7 as well as loaded coplanar electrodes as shown Fig. 8 below (i.e. including phase shifter diode). The frequency range was set to be between 0.1 GHz and 40 GHz, the latter being the upper frequency limit of the measurement equipment. The equipment response all the way up to the probe tip was first normalised out of the measurements via a standard calibration

#144401 - $15.00 USD Received 18 Mar 2011; revised 17 May 2011; accepted 25 May 2011; published 2 Jun 2011

process, and then a reverse bias of 3 V was applied to the device. The measurements were performed on two chips, the first on a dummy chip of the same configuration but with no doping or vias.

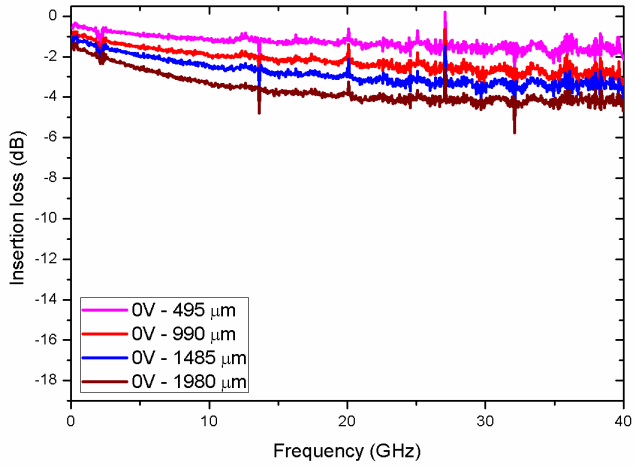

Fig. 8. S_{21} measurements showing the transmission of the coplanar waveguides for an unloaded coplanar waveguide on a chip where no doping or via are present.

These are referred to in this text as unloaded transmission lines. The second experimental measurements were carried out on the diodes together with the electrodes, and these are referred to as loaded transmission line measurements.

Unloaded transmission line measurements (Fig. 8) show that the transmission over the measured range is within –6 dB for all line lengths up to 1980 micrometers.

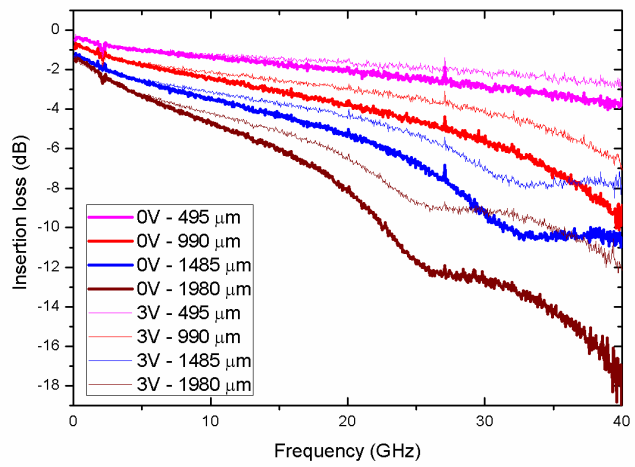

Fig. 9. S_{21} measurements showing the transmission performed on loaded coplanar waveguides which contains a phase shifter diode. Measurements were performed at 0V and 3V reverse bias. The coplanar waveguide transmissions are measured for lengths from 490 micrometers up to 1980 micrometers where the phase shifter diodes are slightly shorter, of length 450, 900, 1350 and 1800 micrometers.

This is not the case when moving to loaded transmission lines (Fig. 9) where the –6 dB roll off point is reached for a CPW length of 980 micrometers, supporting a 900 micrometers long diode at 40GHz. Similarly the electrical 6 dB roll off frequency is at 27 and 17 GHz respectively for CPW lengths of 1485 and 1980 micrometers (supporting diodes of length 1350 micrometers and 1800 micrometers). It is also necessary to note that the RF losses are

#144401 - $15.00 USD Received 18 Mar 2011; revised 17 May 2011; accepted 25 May 2011; published 2 Jun 2011

higher if no reverse bias is applied as shown in Fig. 9. This additional loss results from two effects; the increase of the diode capacitance which causes an enhancement in the resistive loss along the CPW as well as an increase of the impedance mismatch increasing microwave reflections. The line reflection (S_{11}) was also measured using the same experimental conditions showing reflection loss below 10 dB up to a bandwidth of 40 GHz for loaded and unloaded lines indicating a good impedance matching to 50 Ohms. The frequency bandwidth roll off of 27 GHz (1485 micrometer long CPW driving a 1350 micrometer long diode) should not limit the 10 Gb/s 'non return to Zero' (NRZ) data, because it supports propagation up to the 4th harmonic (25GHz) of the 5 GHz square signal. It should also be sufficient to support the fundamental component of the 20 GHz square signal of 40 Gb/s NRZ data.

The IV and s-parameters measurements show that the optical modulation could be performed in a reverse voltage range from 0 to 6 V, where the optical modulation bandwidth would not be limited by the CPW electrodes for either 10 Gb/s or 40 Gb/s operation, for the device lengths up to 1485 micrometers. Above 1485 micrometers the electrode loss would limit the operation for the 20 GHz component of the 40 Gb/s NRZ signal but would still be acceptable for 10 Gb/s operation. To demonstrate this, data rate measurements were then performed for a CPW line of length 1485 micrometers driving a 1350 micrometer long phase shifter diode.

The data rate measurements were performed using a 40 Gb/s PRBS generator (and DEMUX to obtain 10Gb/s), fed into a microwave amplifier providing 6.5 V_{pp} and 6 V_{pp} swings at 10 Gb/s and 40 Gb/s respectively. The phase shifter was reverse biased at −3 V using a bias tee and the CPW electrode was terminated by a DC block and a 50 Ohm load. A collimated polarisation controlled CW beam was used to feed the modulator, and the modulated laser beam coming out of the chip was fed into an EDFA followed by a band pass tuneable filter and finally measured by a Digital Communications Analyser (DCA) for which the optical head has a bandwidth of approximately 65 GHz. Prior to each measurement, the DCA optical input was calibrated to the background noise of the EDFA to provide an accurate result of the modulation depth (extinction ratio). The measurements were performed at ~1557 nm for both polarisations, where the extinction ratio of the eye was measured to give the maximum value which intrinsically corresponds to the maximum extinction ratio measured at DC shown in Fig. 4 and 5 for both TE and TM polarisations. Figures 10 and 11 show the optical eye diagrams at 10 Gb/s for both polarisations, and for each, an extinction ratio of approximately 7.3 dB is obtained.

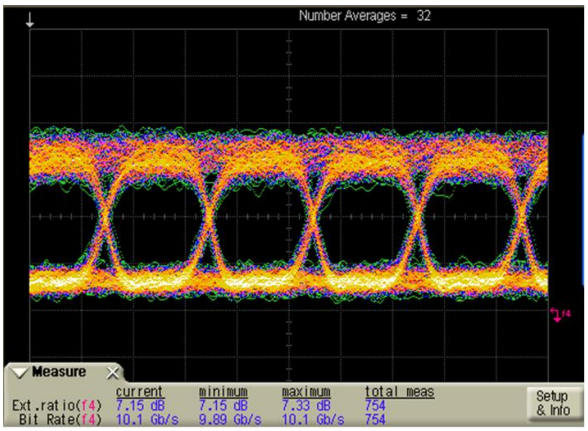

Fig. 10. Eye diagram for a 1350 micrometers long device measured at 10 Gb/s, and at a wavelength of ~1557 nm for TE polarisation. The extinction ratio is approximately 7.3 dB.

#144401 - $15.00 USD Received 18 Mar 2011; revised 17 May 2011; accepted 25 May 2011; published 2 Jun 2011

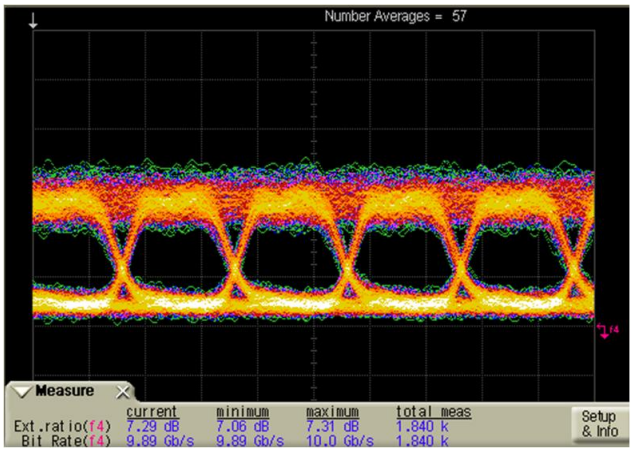

Fig. 11. Eye diagram for a 1350 micrometers long device measured at 10 Gb/s, and at a wavelength of ~1557 nm for TM polarisation. The extinction ratio is approximately 7.3 dB

Measurements at the same wavelength were also performed at 40 Gb/s for TM and TE polarisations as shown in Fig. 12 and 13. Here again the extinction ratios achieved are similar for both TM and TE polarisations, at 6.5 dB. The measurements performed here demonstrate the maximum obtainable extinction ratio for both polarisations; this is however, at the expense of the insertion loss which is in the order of 25dB. It is important to note that for this device the extinction ratio at quadrature is similar to the one measured for TE by [4] at 1dB as indicated by Figs. 3 and 4 with an insertion loss of about 17dB. Hence a trade off can be found between insertion loss and extinction ratio depending on the requirements.

The experimental setup is limited to a bandwidth of 40Ghz, intrinsic to the connectors, cables and probes used in the measurement. In the case of the 10 Gb/s signal a sharp rise and fall time shows that frequency components higher than the fundamental are supported by the diode. In the case of the 40 Gb/s signal only the fundamental 20GHz signal is supported ultimately affecting in part, the shape of the 40 Gb/s NRZ eye diagram. Nevertheless the attenuation of the modulation amplitude is minimal, less than 1 dB difference between the 10 Gb/s signal and the 40Gb/s signal, showing very little difference in roll off between the two frequencies of operation. This indicates that the roll off frequency is much higher than 20 GHz and is probably limited by the electrode response for which the roll off was measured at 27 GHz.

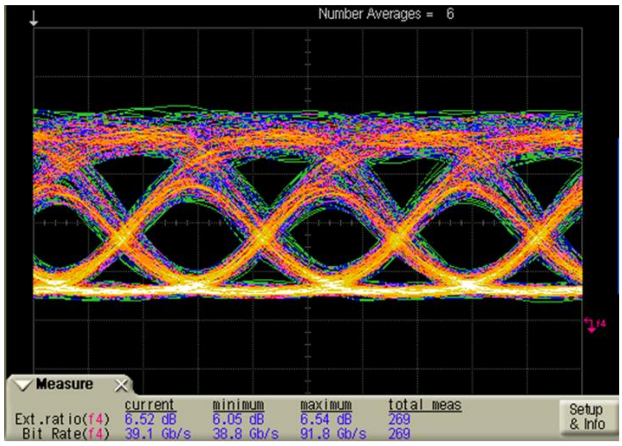

Fig. 12. Eye diagram for a 1350 micrometers long device measured at 40 Gb/s, and at a wavelength of ~1557 nm for TE polarisation. The extinction ratio is approximately 6.5 dB.

#144401 - $15.00 USD Received 18 Mar 2011; revised 17 May 2011; accepted 25 May 2011; published 2 Jun 2011

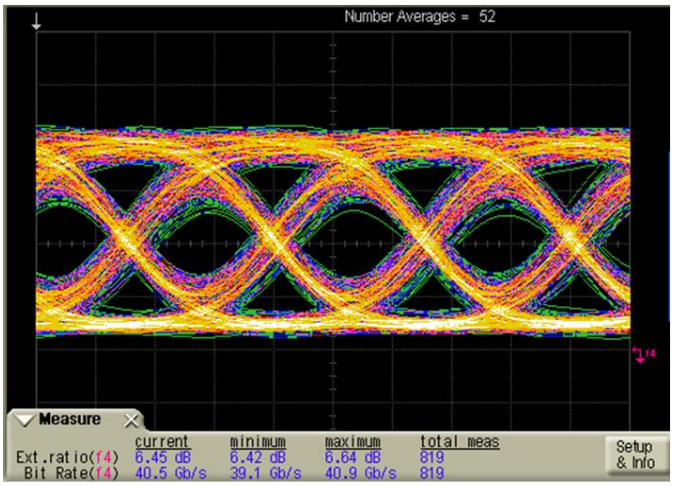

Fig. 13. Eye diagram for a 1350 micrometers long device measured at 40 Gb/s, and at a wavelength of ~1557 nm for TM polarisation. The extinction ratio is approximately 6.5 dB.

4. Power consumption

It is also important to calculate the power consumption of the modulator devices [17]. In order to do so the input voltage was measured at the first harmonic frequency of operation, which is 5 GHz for 10 Gb/s and 20 GHz for 40 Gb/s. Taking into account that the input peak-to-peak voltage will be driven into a 50 Ohm load at the end of the coplanar electrode line, one can assume in the first instance, that this load is part of the modulator. For a 10 Gb/s signal, the input voltage is 6.5 V which in a 50 ohm system represents a 130 mA of current consumption in the load (or 845 mW of power). If we convert this into the conventional figure of merit, of energy (joules) per bit, a figure of 21.1 pJ/bit is obtained for a 10 Gb/s. Now if the same calculation is performed for a 40 Gb/s signal for which the input swing voltage is 6V, we obtain a current of 120 mA (or 720 mW of power) which translates into 4.5 pJ/bit.

An alternative common method of evaluating power consumption is to use the relationship $E = CV^2/4$ (e.g [17].), but this only takes into account the energy required to charge and discharge the capacitance of the device. To do this the capacitance of the line was measured at a reverse bias of 3 volts and at 10 MHz giving a value of 410 fF. This value provides a worst case scenario as the capacitance of the diode will decrease with increasing frequency. The NRZ energy per bit is therefore < 3.7 pJ/bit which for a 40 Gb/s signal operating at 20 GHz is consistent with the value stated above.

5. Conclusion

To summarise, a 1350 micrometers long phase shifter has been demonstrated capable of producing data transmission at both 10 and 40 Gb/s with an extinction ratio up to 6.5 dB at 40 Gb/s for both TE and TM polarisations. This, coupled with a power consumption of 4.5 pJ/bit at 40 Gb/s together with the broadband characteristics of MZI structures, shows the potential for the device to satisfy the high speed requirements of future interconnects. Furthermore this device shows a significant improvement over the Intel devices [4] in terms of power consumption and polarisation independence. Futhermore, the CMOS fabrication process is based on a series of self-aligned implants which simplifies the process and hence offers potential improvements in process reliability and yield. The on-chip loss of 15 dB is much higher than expected, and is significantly impacted by the higher than expected waveguide loss. In this device the phase shifters themselves are only responsible for ~6 to 7 dB of the loss, hence further iterations of the device should show a reduced waveguide loss towards a total insertion loss figure closer to 7dB.

#144401 - $15.00 USD Received 18 Mar 2011; revised 17 May 2011; accepted 25 May 2011; published 2 Jun 2011

It is also interesting to note that an active length of only 700 micrometers would be required if the modulator was driven in a push-pull scheme, which further increases the possibility of high integration packing density for these devices as well as decreasing both the optical loss due to the phase shifter and the microwave loss by a factor of two. This further increases the possibility of reaching even higher data rates and could contribute to terascale computing applications as, at the demonstrated data rate of 40Gbit/s, only 25 of these devices are required to provide an aggregate data rate of 1 terabit per second for future multi core platforms.

Acknowledgements

The research leading to these results has received funding from the UK EPSRC funding body under the grant UK Silicon Photonics. The Authors would also like to thanks the Epixfab platform, CEA-Leti for device fabrication and in particular Dr Jean Marc Fedeli. We are also grateful to Dr Goran Mashanovich for useful discussions and Dr William Headley for preparation of experiments.

#144401 - $15.00 USD Received 18 Mar 2011; revised 17 May 2011; accepted 25 May 2011; published 2 Jun 2011